FlatChem 55 (2026) 100995

Contents lists available at ScienceDirect

FlatChem

journal homepage: www.sciencedirect.com/journal/flatchem

Molecular layering and CO_2 selectivity in graphene-supported natural deep eutectic solvent films: An *in-silico* investigation

Sara Rozas [a,b], Nuria Aguilar [a], Pedro A. Marcos [c], Alfredo Bol [b,c], Santiago Aparicio [a,b,*]

[a] Department of Chemistry, University of Burgos, 09001 Burgos, Spain
[b] International Research Centre in Critical Raw Materials-ICCRAM, University of Burgos, 09001 Burgos, Spain
[c] Department of Physics, University of Burgos, 09001 Burgos, Spain

ARTICLE INFO

Keywords:
CO_2 capture
Flue gas
Deep eutectic solvents
Thin films
Graphene
Quantum chemistry
Molecular dynamics

ABSTRACT

A multiscale computational study was conducted to investigate graphene-supported thin films composed of a natural deep eutectic solvent (NADES) formed by menthol and decanoic acid (MENTH:DA), with a focus on applications in sustainable CO_2 capture. Density functional theory (DFT) and molecular dynamics (MD) simulations were employed to elucidate interfacial structuring, molecular interactions, and gas adsorption behavior. DFT results indicated a strong interaction between decanoic acid and the graphene surface (−35.88 kJ/mol), characterized by a parallel orientation that maximizes van der Waals interactions. In contrast, menthol displayed weaker adsorption energies (−5.15 kJ/mol) and a predominantly perpendicular orientation. MD simulations revealed the formation of distinct adsorption layers, with decanoic acid enriched in the first layer and menthol in the second, while the NADES hydrogen-bonding network remained largely intact. CO_2 exhibited preferential adsorption over flue gas components (N_2, H_2O, O_2), with substantial accumulation in both the first and second interfacial layers. Approximately 50% of the CO_2 content from flue gas mixtures was retained within the structured region. Adsorption performance was found to be largely independent of temperature (303−323K) and NADES film thickness (20–50 Å). These results provide fundamental insight into NADES–graphene interactions and highlight the potential of type V, naturally derived deep eutectic solvents as selective and environmentally benign materials for CO_2 separation technologies.

1. Introduction

The climate emergency has emerged as one of the most pressing socio-technological and economic challenges of our time. Anthropogenic CO_2 emissions, primarily resulting from the combustion of fossil fuels in power generation, transportation, and heavy industries, have significantly contributed to the rise in atmospheric CO_2 levels, reaching a concentration of 429.15 ppm. [1]. This historical maximum of CO_2 atmospheric concentration have led to the increase of Earth's surface temperature, ocean acidification or ecosystems collapse.In this context, CO_2 capture technologies have been proposed as a suitable approach both for capturing from emission sources as well as for direct atmospheric capture [2]. Among the proposed capturing technologies, Deep Eutectic Solvents (DES) have recently emerged as a suitable alternative, considering their environmentally friendly nature, low toxicity and low cost, as well as their remarkable physicochemical properties and excellent CO_2 affinity [3]. For example, amine-functionalized DESs have exhibited outstanding CO_2 capture performance, primarily through chemisorption mechanisms, achieving high gravimetric capacities. Systems such as triethylenetetramine chloride: diethylene glycol have been reported to reach up to 1.42 mol CO_2 per mol of DES, which weighty overcome the widely used toxic monoethanolamine yields [4]. However, recent research is increasingly focused on greener alternatives, particularly type V DESs, which consist solely of non-ionic organic hydrogen bond donors and acceptors. These systems offer enhanced tunability and eliminate the need for ionic components, aligning with sustainability goals. Notable examples include DESs based on monoterpenoid compounds such as carvone: menthol and cineole: lactic acid, which have demonstrated CO_2 absorption capacities of 0.96 [5] and 0.95 [6] mol CO_2 per mol of DES, respectively.

The adsorption of DES on graphene surfaces has recently attracted increasing attention due to their potential applications in diverse fields such as electrochemistry [7,8], photothermal energy conversion [9] and tribology [10], with particular interest in their role as platforms for

* Corresponding author at: Department of Chemistry, University of Burgos, 09001 Burgos, Spain.
E-mail address: sapar@ubu.es (S. Aparicio).

https://doi.org/10.1016/j.flatc.2026.100995
Received 22 July 2025; Received in revised form 19 December 2025; Accepted 8 January 2026
Available online 9 January 2026

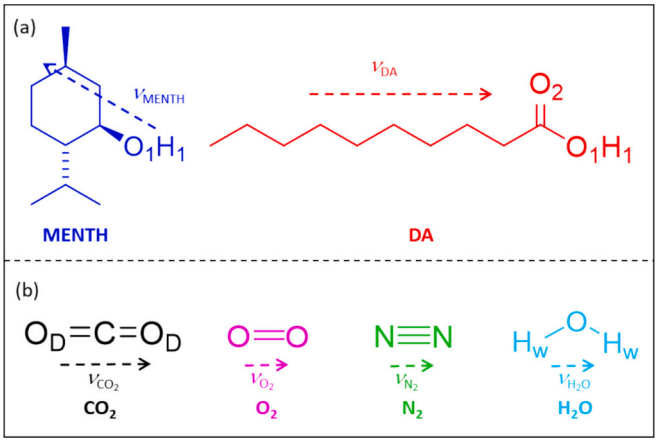

Fig. 1. (a) DES HBA and HBD and (b) gas molecules involved in this work. Dashed arrows depict vectors used for defined molecular orientations in following figures.

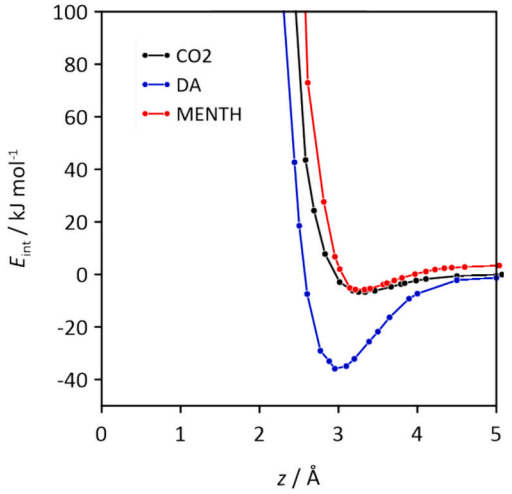

Fig. 2. Counter Poise corrected interaction energies, E_{int}, as a function of distance to the GRA surface, d_z (as defined in Fig. S2) of MENTH, DA and CO_2 molecules on top of GRA surface calculated at wB97X def2-SVP def2/J theoretical level. These curves are obtained from shifting upward or downward the optimized structures reported in Fig. S2.

Table 1
GRA – MENTH/DA/CO_2 interaction energy, E_{int}, equilibrium distance to GRA surface, d_z, and charge transfer calculated after the geometry optimization, Δq, from DFT calculated at wB97X def2-SVP def2/J theoretical level.

i	E_{int} / $kJ \times Mol^{-1}$	d_z	Δq_{GRA} / e	Δq_i / e
MENTH	−90.02	3.50	−0.038	0.038
DA	−120.75	2.95	−0.024	0.024
CO_2	−91.04	3.18	0.005	−0.005

novel nanofluids. Previous few studies have explored these interactions at the molecular level. For instance, M. Shakourian-Fard et al. employed density functional theory (DFT) calculations to investigate the nature of interactions between graphene flakes and various choline chloride-based type III DESs (this DES type consists of an ionic pair and a hydrogen bond donor) [11]. Their results highlighted the significant role of the chloride anion in governing the interfacial behavior. In a separate study, M. Atilhan et al. conducted DFT calculations and molecular dynamics (MD) simulations to elucidate the nanowetting behavior of choline chloride-based type III DES on graphene surfaces [12]. They reported localized structural rearrangements of the DES molecules near the graphene interface, while noting that the overall hydrogen-bonding network characteristic of the DES remained largely intact. Furthermore, the same group demonstrated that the adsorption of three mixed choline chloride-based DES on 2D materials, including graphene, leads to a pronounced densification of the first adsorbed layer. This densification is accompanied by an enrichment of choline chloride and the hydrogen bond donors at the graphene-DES interface. Despite this advances, molecular level studies of DES adsorption phenomena remain scarce. Moreover, there is a notable lack of investigation involving emerging type V DES or natural deep eutectic solvents (NADES). Unlike type III DESs, type V systems are composed of two organic, naturally occurring components -one acting as hydrogen bond donor (HBD) and the other as hydrogen bond acceptor (HBA)- and do not contain ionic species. The study of such natural NADES is of particular interest, not only from a sustainability perspective, but also because the absence of ionic components raises fundamental questions about their interaction mechanisms with graphene surfaces.

In this work, we go a step further and analyze a natural deep eutectic solvent based on MENTH – DA in the formation of thin films on graphene (GRA), *i.e.* leading to membranes assemblies for carbon capture purposes from flue gas sources. The nature and properties of these materials were studied using *in silico* simulations: based on quantum mechanics, using DFT, and classical mechanics, using MD methods. The main goal of this investigation is to understand, on the one hand, NADES – GRA interfacial behavior, and on the other hand, complex thin layers performance on CO_2 adsorption. For the latter, pure carbon dioxide gas and a flue gas model resembling industrial emissions, were considered. Thus, a computational approach on GRA covered by MENTH:DA NADES thin film has been accomplished, shedding light on a novel assembly (membranes based on 2D support) leading to eco – friendly materials for suitable and techno-economically viable CO_2 capture technologies.

This study directly contributes to the understanding of 2D material–liquid interfaces, offering molecular-level insights into graphene-supported solvent structuring and gas separation mechanisms relevant to environmental and energy applications.

2. Materials and methods

DFT calculations were done using the latest Orca software version 6.0.1 [13] and employing wB97X functional [14] and def2-SVP [15] def2/J [16] basis set. Geometry optimized structures of MENTH, DA, CO_2 molecules (Fig. 1), and MENTH-DA NADES complexes were taken from our previous work [17] and reoptimized at the considered theory level. A graphene nanosheet containing 178 carbon atoms (with edge carbons hydrogen-saturated) of 22 × 22 Å dimensions (Fig. S1) was used for all the DFT calculations. Molecular species were placed on top of graphene flake and structural relaxation was done using conjugate gradients. Several initial configurations were calculated for each system according to molecular geometry. Interaction energies, E_{int}, were calculated using Eq. (1).

$$E_{int} = E_{i-GRA} - E_i - E_{GRA} \quad (1)$$

where i stands for MENTH, DA or CO_2, $E_{i\text{-}GRA}$ for the counter poise corrected [18] energy for the system formed by the molecular species adsorbed on graphene, E_i for the energy of the isolated MENTH, DA and CO_2, and E_{GRA} for the energy of the clean graphene surface. Charge transfer between molecular species and the graphene flake were calculated by assessing the difference of the charge on each specie before and after adsorption, Δq_i (i = GRA, MENTH, DA and CO_2), as provided by Hirshfeld method [19]. The topology of adsorption interactions was analyzed considering both electrostatics and VdW type molecular interactions, employing Non-Covalent Interaction (NCI [20]) analysis and electrostatic potential (ESP) isosurfaces, respectively, as implemented in the MultiWFN software [21].

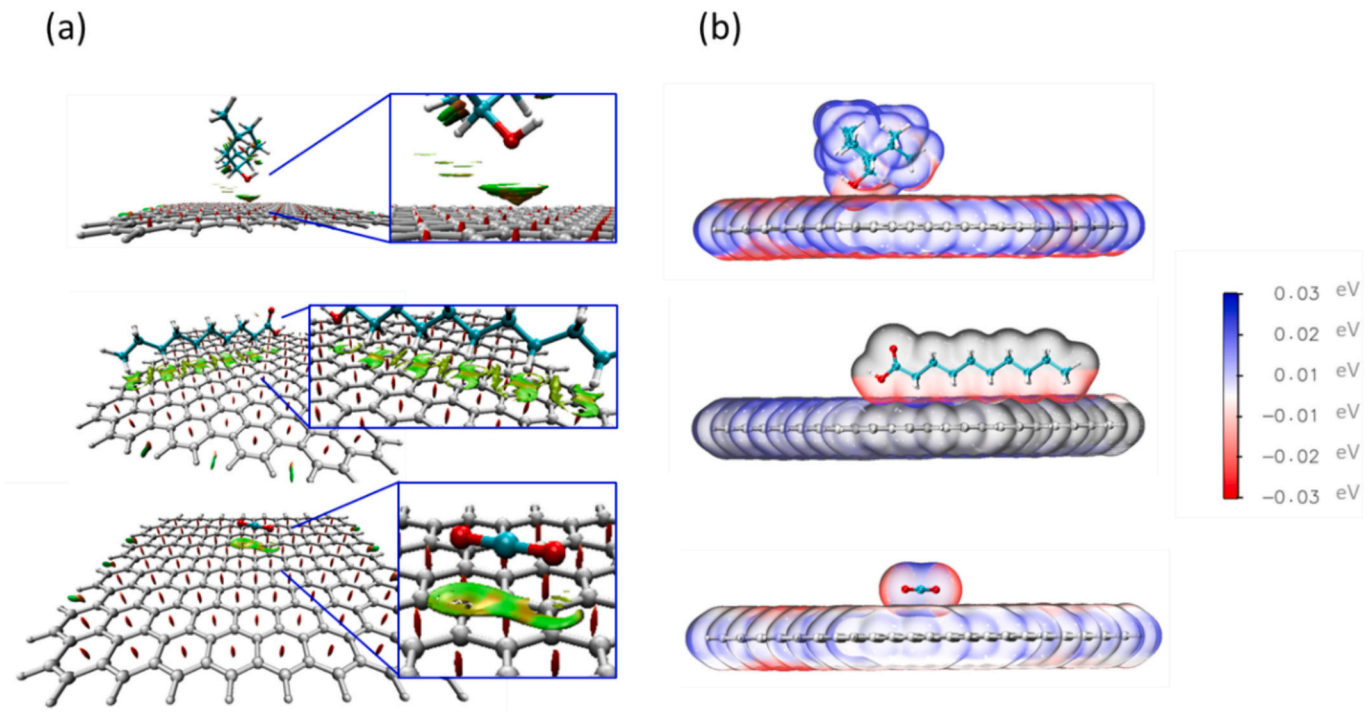

Fig. 3. (a) Non-Covalent Interactions (NCI) analysis and (b) total Electrostatic potential (ESP) isosurface of the individual components for -from top to bottom- GRA – MENTH, GRA – DA and GRA – CO_2.

MD simulations were carried out using MDynaMix v.5.2 software [22]. The force field parameters of NADES molecules employed in this investigation is outlined in Table S1 (Supplementary Information) and is based on parameters derived from the Merck Molecular Force Field, as sourced from the SwissParam [23] database. Notably, atomic charges were determined using ChelpG charges model [24], which were obtained from DFT calculations of isolated monomers. The force field was validated in the previous work [17]. Lennard – Jones parameters for graphene sheets, Table S1-S8, were also previously reported [25]. Gas molecules were described by specific potential models [26,27]. Initial simulation boxes were constructed according to previously reported fluid density [17] using the Packmol program [28]. Different number of MENTH and DA molecules corresponding to the targeted DES thickness (20, 30, 40 and 50 Å) and graphene sheet side length were considered (see Table S9a in the Supporting Information for more details). A graphene sheet, adopting an armchair configuration and comprising 1500 carbon atoms, was constructed with side dimensions of 62 × 62 $Å^2$ and aligned with the *xy* plane. The DES boxes were then positioned 2 Å above the graphene surface, establishing an interface parallel to the *xy* plane. Flue gas, containing 70% N_2, 15% CO_2, 10% H_2O and 5% O_2, and CO_2 pure gas boxes were constructed with Packmol according to graphene sheet side length and considering 150 Å thickness in the *z* direction. The gas boxes were then positioned 2 Å above the DES surface, establishing an additional interface parallel to the *xy* plane (Table S9b and S2c). Periodic boundary conditions (PBC) were imposed in all spatial directions, with the system dimension along the *z*-axis ensuring the formation of *a)* DES – vacuum, *b)* DES – CO_2 and *c)* DES – flue gas interface above the DES liquid layers, as depicted in Table S9. 303 K, 313 K and 323 K temperature and 1 bar pressure conditions were considered. The MD simulations consisted of a 30 ns in the canonical ensemble (NVT) for equilibration at considered Kelvin and the corresponding pressure. The Nose-Hoover method [29] was employed to control pressure and temperature during these simulations. For the numerical integration of equations of motion, the Tuckerman-Berne [30] double time step algorithm was applied, featuring time steps of 3 femtosecond (fs) and 0.3 fs for long- and short-time steps, respectively. To account for electrostatic interactions, the Ewald method [31] was implemented with a cut-off radius of 10 Å. Lennard-Jones interactions were truncated at 10 Å, and Lorentz-Berthelot mixing rules were employed for cross terms in the potential functions. Post-simulation trajectory analysis was conducted utilizing the TRAVIS [32] and VMD programs [33], enabling the extraction of insights into the structural characteristics of intermolecular forces within the NADES systems under investigation.

3. Results

3.1. Density functional theory calculations: short-range interactions

The intermolecular interactions of MENTH and DA, as well as CO_2, with GRA surface were firstly analyzed using DFT. Different molecular orientations (*i.e.*, hydroxyl group of MENTH and carboxylic head of DA oriented towards and away from GRA surface) and spatial arrangements (parallel and perpendicular to GRA surface) were evaluated (Fig. S2), and the most stable configurations (lowest interaction energy, E_{int}, values), were further analyzed. The interaction of MENTH with GRA surface is characterized by the orientation of the hydroxyl group, with the oxygen atom being placed 3.50 Å above GRA ring, Fig. S3. In contrast, DA interacts with the GRA surface by lining up along GRA flake surface, promoting effective VdW interactions, with the alkyl hydrogen atoms being placed 2.95 Å above the C—C GRA region, Fig. S3. The interaction energy between MENTH-GRA and DA-GRA pairs, was

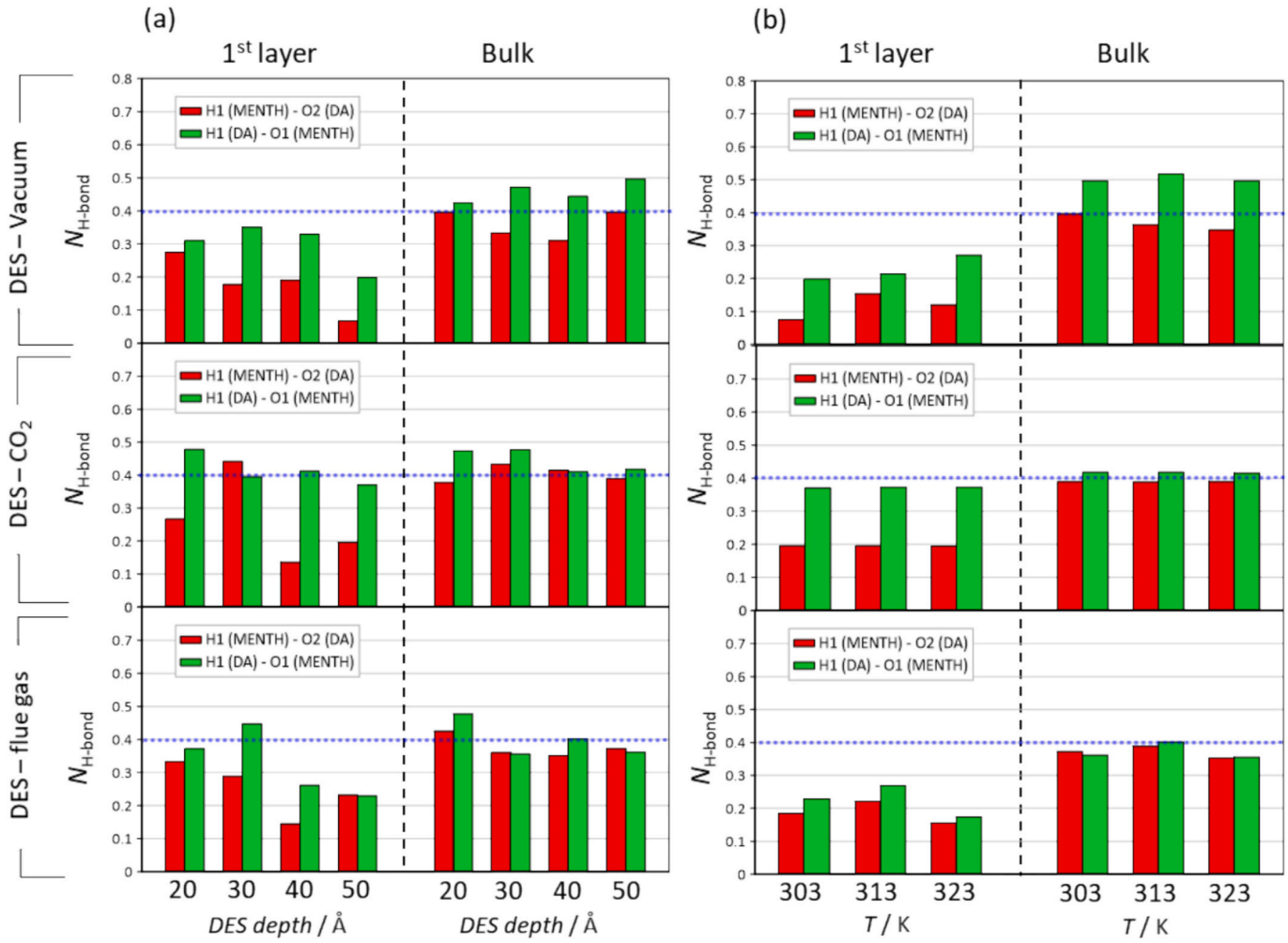

Fig. 4. Average number of MENTH: DA hydrogen bonds, $N_{\text{H-bonds}}$, on top of GRA surface. Values are reported for molecules in the first adsorbed layer ($z < 6.5$ Å) and in the bulk region (11 Å $< z < z_{\text{DES}}$). The averages are calculated by dividing the total number of hydrogen bonds by the total number of donor molecules. Results from MD simulations at (a) 303 K and different DES depth and (b) 50 Å DES depth and different temperatures. Donor-acceptor distance and angle of 3.5 Å and 30° were used as cutoffs for hydrogen bond definition. Blue dotted line refers to average $N_{\text{H-bonds}}$ value for neat bulk DES from reference [17]. (For interpretation of the references to colour in this figure legend, the reader is referred to the web version of this article.)

calculated as a function of distance to the surface, z, Fig. 2. The curves reported in Fig. 2 were built by enlarging and shortening the distance between MENTH or DA and GRA surface starting from the optimized structures reported in Fig. S3 (Table 1 for data), and maintaining the remaining parameters of the cluster constant. Results in Fig. 2 reveal energy minimum of −5.15 kJ × mol^{-1} and -35.88 kJ × mol^{-1} for the interaction of MENTH and DA with GRA surface, respectively. DA – GRA interaction energy is remarkably larger, and in agreement with other small organic adsorbates [12,34]. These values are consistent with strong DA adsorption, indicating that the interaction between the DA and GRA, nearly planar adsorption geometry with the presence of COOH group, is significantly stronger than that with MENTH. This suggests that the overall interaction of NADES with the GRA surface may be primarily driven by the strong adsorption of DA, while MENTH contribution play a secondary role. DA-GRA~~s~~ strong interaction is further supported by a slight charge transfer from DA to GRA at the energy minimum ($\Delta q_{\text{GRA}} = -0.024$ e), as determined by the Hirshfeld method, resulting in a net charge of +0.024 e on the DA, Table 1. The charge transfer is slightly larger in the MENTH – GRA interaction, $\Delta q_{\text{GRA}} = -0.038$ e, with a net charge of +0.038 e on the MENTH. The larger charge transfer in the MENTH – GRA system~~,~~ might be due to the direct contact established between the hydroxyl group (more polarized than the ring region) with the GRA surface. These charge transfer values, which are in agreement with other non-ionic species interactions with GRA flakes [12], play a minimal role in NADES components adsorption, exemplified by the high E_{int}.

The interaction of CO_2 with GRA was also characterized, and distinguished by lying parallel to the GRA surface, maximizing VdW interactions, with the carbon atom of the gas molecule being placed 3.18 Å above the C—C GRA region, Fig. S3. Moreover, moderate interaction ($E_{\text{int}} = -6.18$ kJ × mol^{-1}, Fig. 2), slightly higher than that for MENTH – GRA, and negligible charge transfer from GRA to CO_2 ($\Delta q_{\text{GRA}} = +0.005$ e, Table 1) was inferred, hinting suitable GRA surface affinity for CO_2 molecules.

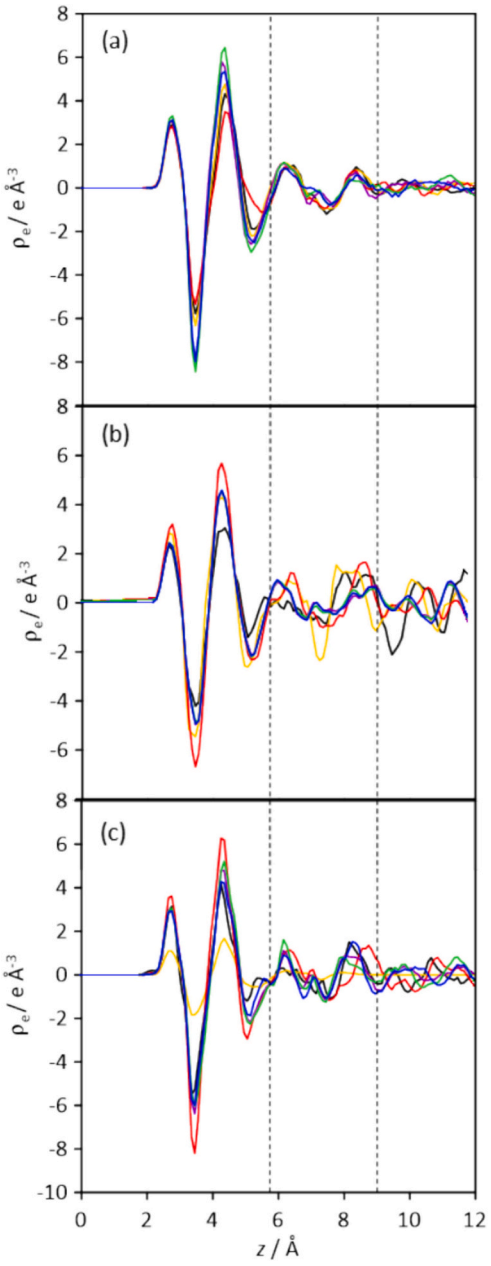

Fig. 5. Total charge density, ρ_e, for the (a) GRA – DES in vacuum, (b) GRA – DES + CO_2 gas and (c) GRA – DES + flue gas systems as a function of the distance, z, to the GRA surface from MD simulations. Only data in the vicinity of the GRA surface ($z < 12$ Å) is reported. Dashed lines show boundaries of the first and second adsorbed layers. Colour code: 303 K and 20 Å (black), 303 K and 30 Å (yellow), 303 K and 40 Å (red), 303 K and 50 Å (purple), 313 K and 50 Å (green) and 323 K and 50 Å (blue). (For interpretation of the references to colour in this figure legend, the reader is referred to the web version of this article.)

Further insights into the intermolecular interactions of MENTH, DA and CO_2 on the GRA nanoflake were obtained using NCI analysis, Fig. 3a. In the case of MENTH molecule, the NCI plot revealed localized green regions corresponding to VdW interactions, primarily at the (MENTH)O1···ring(GRA) site. For the DA, NCI indicates localized VdW interactions along the alkyl chain (DA)H_{alkyl}···C(GRA) and (DA)C_{alkyl}···C (GRA) sites. Lastly, the CO_2 system displays large VdW interactions, as evidenced by the presence of light green regions along the (CO_2)C···C-C (GRA) and (CO_2)O···ring(GRA) contacts, Fig. S3 and Fig. 3. To complement the NCI analysis, ESP isosurfaces were analyzed to provide a more comprehensive topological characterization of the NADES components on GRA surface, Fig. 3b. The ESP isosurfaces measure the electrostatic interaction energy provided by VdW surfaces of individual species. The interpenetration of VdW surfaces and the resulting electrostatic complementary effect are observable through regions of positive (blue) and negative (red) ESP. Red (negative potential) regions of MENTH, DA and CO_2 molecules ESP inserted in blue (positive potential) regions of GRA ESP denote VdW interactions between MENTH/DA/CO_2 and GRA. These results reveal that, in all systems, electrostatic interactions occur between the adsorbate and GRA surface.

These findings are based on single-complex adsorption models. To assess collective effects from the liquid phase adsorbed on graphene, further analysis using classical molecular dynamics simulations is presented in the following section. Two phenomena are studied under classic MD simulations: *i)* NADES physicochemical properties after lining on graphene surface (GRA-DES-vacuum setup, Fig. S2a), and *ii)* CO_2 absorption performance of NADES lining graphene (GRA-DES-CO_2 setup, Fig. S2b, and GRA-DES-flue gas setup, Fig. S2c).

3.2. Molecular dynamics simulations: Long-range interactions

3.2.1. NADES lining on graphene surface

The adsorption behavior of NADES on GRA surfaces is described as number density profiles, ρ, for the center-of-mass of MENTH and DA molecules along z axis, Fig. S4 and S5. The GRA surface significantly perturbs DES structure up to 10.5 Å away. The DES region above GRA is segmented into three zones—first layer (3 to 6.5 Å), second layer (6.5 to 10.5 Å), and a bulk region—. ρ values showed low dependency on NADES aggregation (20 to 50 Å depth) or heating (303 to 323 K), therefore, no effects on adsorption structuring were revealed by solvent lining and heat conditions. The first peak height of the ρ plots represents the adsorption distance of the center-of-mass of MENTH and DA to GRA surface in the first layer, Fig. S4a and S5a. These values are in fair agreement with values reported in the previous section (~ 3.5 and ~ 2.95 Å from GRA surface for MENTH and DA, respectively, considering that DFT distances were not related to center-of-masses), Fig. S3. Table S10 lists the molecular populations in the first adsorption layer. The first adsorbed layer contains a higher molecular density than the bulk for all DESs. While this layer is formally defined from 0 to 5 Å (with 0 Å at the GRA surface), Fig. S4 shows molecular accumulation predominantly within the 3–5 Å range. Furthermore, the DA/MENTH ratio in the first layer exceeds 1.0 ($N_{DA} > N_{MENTH}$), indicating a relative MENTH deficit. This imbalance is offset in the second layer, where DA/MENTH ratios are lower than 1.0, Fig. S4 and S5. The second layer serves as a transitional zone between the structured adsorption region and the bulk-like domain. These findings support the multilayer structuring of DESs on GRA.

NADES behavior on GRA surface is further assessed through the number of hydrogen bonds, described from the average number of hydrogen bonds, $N_{H\text{-}bond}$, per acceptor molecule. In a previous work, MD simulations of neat bulk NADES revealed H1(MENTH)-O2(DA) and H1(DA)-O1(MENTH) hydrogen bonds, labels as in Fig. 1, as the major contributions to MENTH-DA interactions upon NADES formation [17]. Precisely, the reported $N_{H\text{-}bond}$ average value for H1(MENTH)-O2 and H1(DA)-O1(MENTH) for 1 MENTH:1 DA bulk system over a wide range of pressure (1 to 40 bar) and temperatures (298 to 323 K) conditions was 0.4. In this work, we report the calculated $N_{H\text{-}bond}$ values for these hydrogen bonds, along the first adsorption layer ($z < 6.5$ Å) and in the

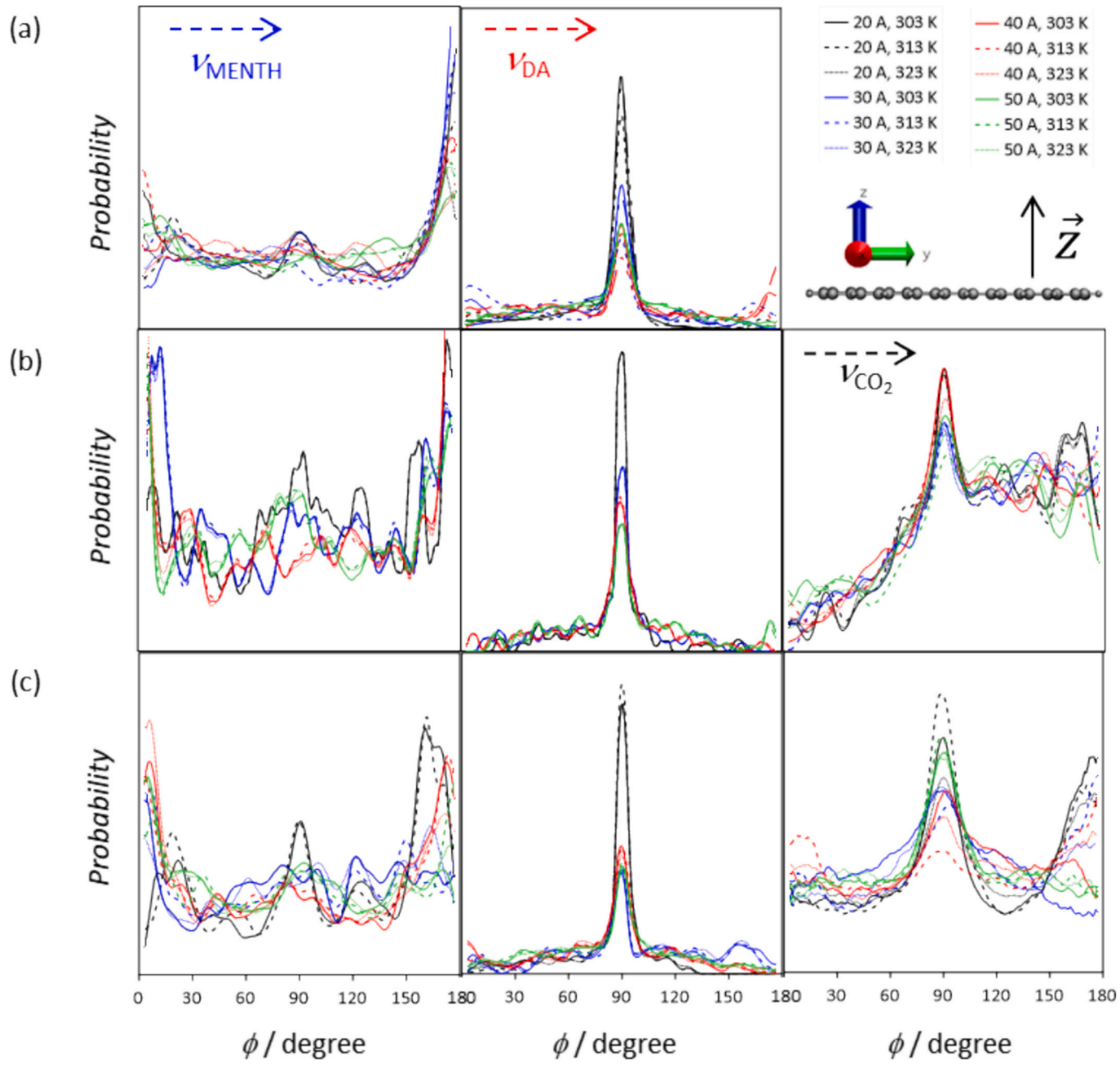

Fig. 6. Angular distribution function plots for the angle, ϕ, formed between a vector perpendicular to the GRA surface ($\vec{z}$) and the MENTH, DA and CO_2 molecular vectors defined in Fig. 1, for (a) GRA – DES in vacuum, (b) GRA – DES + CO_2 and (c) GRA – DES + flue gas systems from MD simulations.

bulk region (z > 11 Å), and its reliance on DES depth and temperature, Fig. 4a and b, respectively. In the bulk region of the adsorbed NADESs, strong hydrogen bonding between hydrogen bond acceptors and donors is characteristic consistent with $N_{H\text{-}bond}$ average values reported for the bulk liquids, Fig. 4. However, this bonding is disrupted upon NADES adsorption on GRA due to densification and molecular rearrangement along the GRA-NADES interface (Figs. S4 and S5). Fig. 4 (blue dotted line as bulk $N_{H\text{-}bond}$ = 0.4 average value reference) compares average hydrogen bond counts of 1st layer adsorbed NADES and pseudo-bulk regions, showing $N_{H\text{-}bond}$ lessening in all hydrogen bond types upon adsorption.

NADES adsorption on GRA modifies the solvent charge distribution near GRA from random distribution in the bulk, to a defined probability distribution in regions close to GRA surface. Fig. 5 shows the spatial charge density profiles along *z* axis, revealing a positively charged region at the upper edge of the first layer, followed by negative and positive charge regions closer to the surface. These features primarily originate from MENTH orientation contributions (Fig. 6), which tend to position with the -OH group (see ν_{MENTH} in Fig. 1) perpendicular to the surface (Fig. S3). Molecular orientation provides information on the

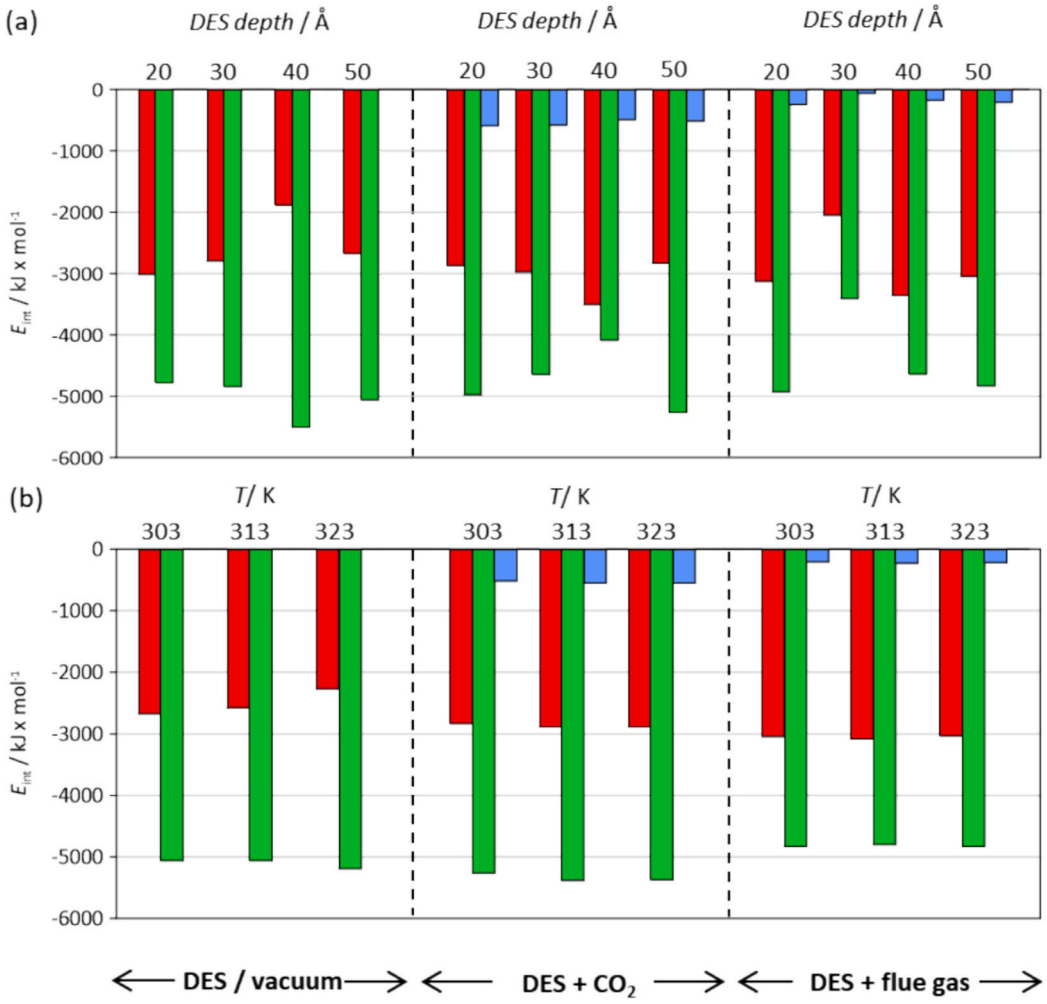

Fig. 7. Interaction energies, E_{int}, for GRA – MENTH (red), GRA – DA (green) and GRA – CO_2 (blue) from MD simulations at (a) 303 K and different DES depths and (b) 50 Å DES depth and different temperatures. GRA – DES, GRA – DES + CO_2 and GRA – DES + flue gas systems were considered. (For interpretation of the references to colour in this figure legend, the reader is referred to the web version of this article.)

solvent structuring on GRA surface. This orientation is assessed by calculating the angle, ϕ, between a molecular vector (defined in Fig. 1) and the surface normal ($\phi = 0°$ means perpendicular, $\phi = 90°$ indicates parallel). Angular probability distributions (Fig. 6) show that MENTH exhibits two preferred orientations—one near 0° or 180° (dominant) and another around 90° (minor)—indicating a mostly perpendicular orientation with slight tilting. DA molecules prefers a parallel orientation to the surface ($\phi = 90°$), consistent with DFT results (Fig. S3). Both charge distribution and molecule orientation remain mostly invariant at different NADES thickness and temperature conditions.

Interaction strengths between NADES components and GRA, quantified as interaction energies (E_{int}), are shown in DES/vacuum section of Fig. 7. As disclosed by DFT calculations, MD results reveal stronger DA–GRA interactions (Table 1), contributing more to the overall interaction energy. DA lying down parallel to GRA surface (Fig. 6) and high concentration in the first layer (Table S10) contributes to a larger DA-GRA contact area, enhancing interaction, whereas lower number of MENTH molecules in lower extent within the close regions to the GRA surface are impeded to interact with GRA surface.

Two main factors govern NADES behavior at the graphene interface: (1) the preference for perpendicular arrangement of MENTH molecules and parallel molecular alignment of DA to enhance graphene interaction, and (2) the preservation of MENTH-DA hydrogen bonding. While surface interactions reconfigure molecular arrangements and weaken hydrogen bonding networks, they do not eliminate them entirely. These structural and energetic modifications are mostly confined within 11 Å of the graphene surface, explaining the layering behavior linked to hydrogen bond disruption.

3.2.2. *CO_2 adsorption into graphene-NADES assembly*

In the final part of this study, we examine GRA-NADES membrane assembly behavior at the interface with gas phases—either pure CO_2 or a model flue gas. This scenario is pertinent for GRA–DES thin layers designed for CO_2 capture *via* physisorption. Number density profiles of CO_2 (pure CO_2 in Fig. 8a and flue gas in Fig. 8b) and its associated gas molecule distributions (pure CO_2 in Table 2 and flue gas in Table 3) after equilibration confirms the adsorption of CO_2 molecules on NADES provided by two adsorption layers. It is critical to consider that the profiles are reported only up to $z = 20$ Å, this range captures the entire crowded volume of the 20 Å film, whereas for the 30 to 50 Å films, CO_2

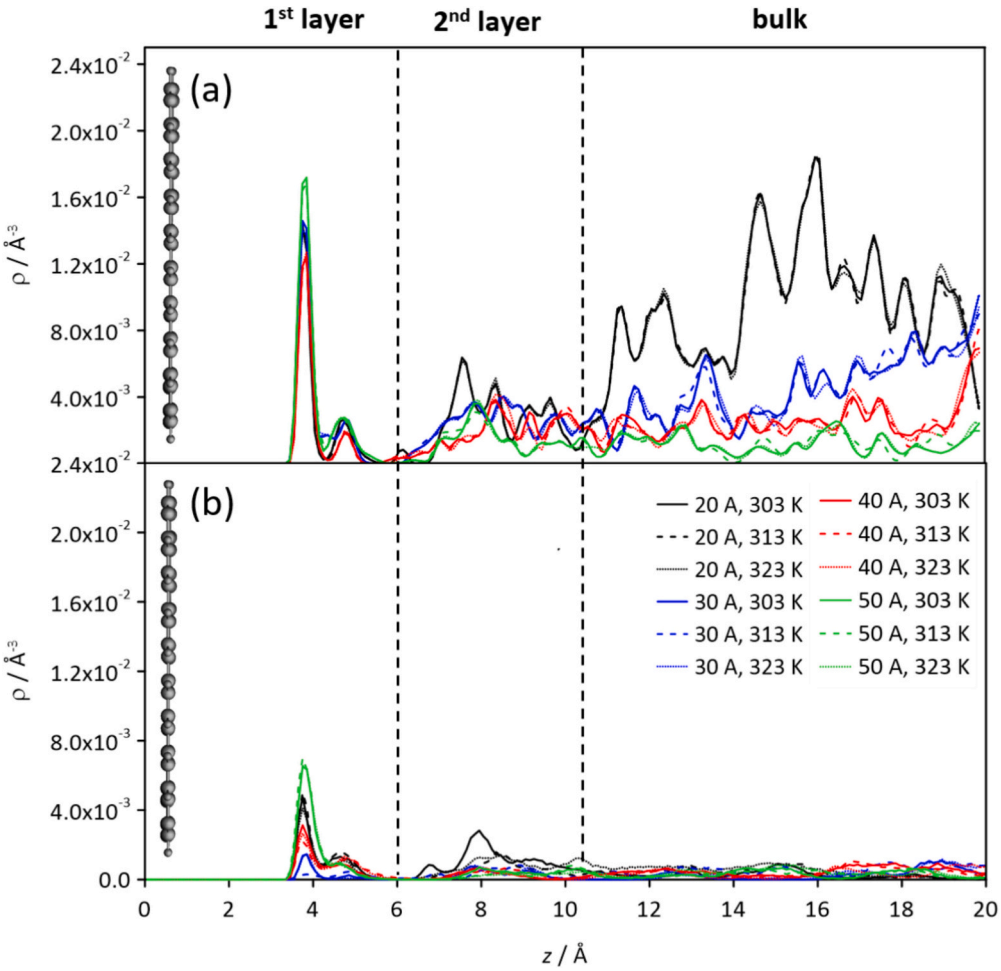

Fig. 8. Number of density profiles, ρ, for the center-of-mass of CO_2 in the (a) GRA – DES + CO_2 and (b) GRA – DES + flue gas systems at the different temperature and DES film depth conditions as a function of the distance, z, to the GRA surface from MD simulations. Only data in the vicinity of the GRA surface ($z < 20$ Å) is reported. Vertical dashed lines represent first and second adsorbed layers.

Table 2
Percentage of CO_2 in the first adsorbed layer ($z < 6.5$ Å), second layer (6.5 Å $< z <$ 11 Å), bulk (11 Å $< z < z_{DES}$) and gas phase ($z_{DES} < z$), where z stands for the distance to GRA surface and z_{DES} for the z at DES – gas interface for GRA – DES + CO_2 systems after MD simulations at the considered DES depth and temperature conditions.

		% CO_2		
DES depth / Å	*T* / K	1st layer	2nd layer	Bulk
	303	5.65	10.47	83.88
20	313	5.65	10.48	83.86
	323	5.65	10.41	83.94
	303	6.27	10.24	83.49
30	313	6.25	10.17	83.59
	323	6.24	10.26	83.49
	303	4.80	7.59	87.61
40	313	4.82	7.67	87.51
	323	4.81	7.66	87.52
	303	7.37	5.33	87.30
50	313	7.37	5.30	87.33
	323	7.36	5.32	87.32

profiles continue in the unplotted bulk region. In the GRA-DES-pure CO_2 systems, CO_2 adsorption is unrelated to NADES aggregation depth or system temperature. There is a significant accumulation of CO_2 gas molecules in the 0–6 Å region, indicating the diffusion of gas molecules through MENTH:DA solvent. Second adsorbed layer is twice as populated with CO_2 molecules as first layer, with the exception of GRA-NADES 50 Å depth for pure CO_2 gas and GRA-NADES 40 and 50 Å for flue gas (Table 2). Despite the second layer being more populated, a lower ordering of the molecules at the second layer is inferred from the weaker peaks in the number density profiles in Fig. 8. Notably, the simulations show that the total amount of available CO_2 molecules was fully adsorbed into the NADES phase. Consequently, the percentage of CO_2 remaining in the gas phase was found to be zero in all investigated cases. In the GRA-DES-flue gas systems, the adsorption behavior is markedly more complex than in pure CO_2 systems due to the competitive interplay between different molecular species. As shown in Table 3, the vast majority of CO_2 molecules were successfully adsorbed into the NADES phase, with only a small fraction remaining in the gas phase ($z > z_{DES}$). The thickness of the NADES film plays a pivotal role in modulating surface accessibility. For the flue gas systems, a significant portion of the captured CO_2 is retained within the first adsorbed layer ($z < 6.5$ Å), although this varies with depth. However, this accumulation is strictly regulated by the presence of water. The data in Table 3 and the density profiles (Fig. 9) highlight a strong competitive effect between CO_2 and H_2O for the primary adsorption sites. Conversely, N_2 and O_2 exhibit much lower affinities for the liquid phase. The competing effect of N_2 is primarily observed in the second adsorption layer (6.5 Å $< z <$ 11 Å), suggesting that N_2 is excluded from the highly ordered primary layer but can partially penetrate the less structured secondary region. Most notably, O_2 shows the lowest adsorption propensity. As evidenced by the high percentage of O_2 remaining in the gas phase (Table 3) and its negligible peaks in the number density profiles (Fig. 9c), O_2 effectively

Table 3
Percentage of flue gas molecules in the first adsorbed layer ($z < 6.5$ Å), second layer (6.5 Å $< z <$ 11 Å), bulk (11 Å $< z < z_{DES}$) and gas phase ($z_{DES} < z$), where z stands for the distance to GRA surface and z_{DES} for the z at DES – gas interface for GRA – DES + flue gas systems from MD simulations at the considered DES depth and temperature conditions.

DES depth / Å		20			30			40			50		
T / K		303	313	323	303	313	323	303	313	323	303	313	323
1st layer	CO_2	27.9	34.1	23.3	4.6	4.4	4.5	17.5	18.5	19.9	28.2	31.2	28.4
	N_2	1.2	2.0	2.1	1.4	1.4	1.5	0.7	0.7	0.7	1.4	1.4	1.4
	O_2	0.0	0.0	0.0	0.0	9.3	0.0	0.0	0.0	0.0	9.6	8.1	9.4
	H_2O	43.3	45.2	41.5	0.0	0.0	0.0	24.0	24.0	24.0	18.9	19.0	20.3
2nd layer	CO_2	46.4	27.3	34.0	7.4	11.6	8.5	9.2	10.3	7.4	11.8	9.9	8.1
	N_2	12.2	12.5	8.9	10.1	10.0	10.3	0.0	0.0	0.0	2.3	1.5	2.2
	O_2	12.5	24.2	6.5	7.8	8.9	9.5	8.4	0.0	0.0	0.2	6.0	0.8
	H_2O	47.6	45.7	49.3	2.6	2.6	2.6	60.2	60.0	60.2	47.7	47.7	46.4
Bulk	CO_2	25.7	38.6	42.6	81.9	77.3	79.7	63.3	59.2	59.3	52.5	51.8	58.1
	N_2	49.0	38.5	30.5	31.3	25.7	26.9	24.2	21.0	24.0	38.0	37.3	34.8
	O_2	62.7	47.3	33.2	49.8	38.1	41.9	38.7	29.8	31.1	49.2	45.0	43.2
	H_2O	9.1	9.1	9.1	97.4	97.4	97.4	15.8	16.0	15.8	33.3	33.3	33.3
Gas phase	CO_2	0.0	0.0	0.0	5.6	6.0	6.7	9.2	10.9	12.4	6.7	6.5	5.0
	N_2	32.9	40.3	52.9	52.1	57.5	55.9	73.4	76.4	73.5	55.1	56.6	58.1
	O_2	22.0	22.9	56.6	39.3	40.0	44.4	48.7	70.2	68.9	40.9	38.6	46.1
	H_2O	0.0	0.0	0.0	0.0	0.0	0.0	0.0	0.0	0.0	0.0	0.0	0.0

acts as an inert spectator.

CO_2 molecules adopt mostly a parallel orientation with respect to the GRA surface regardless of NADES depth and temperature (Fig. 6b for pure CO_2 and 6c for flue gas), maximizing VdW interactions —especially the CO_2 flue gas—, although there is also non-negligible probability distribution at the ϕ corresponding to the molecule to stay perpendicular to the GRA surface ($\phi = 0°$). The energetic driving forces governing adsorption were elucidated by analyzing the interaction energies at the GRA interface (Fig. 7) and within the solvent matrix (Fig. 10). At the graphene interface, the interaction energies are dominated by the strong adhesion of the NADES components to the surface. A critical distinction arises regarding the adsorbate: in the GRA-NADES-pure CO_2 systems, we observe a moderate but distinct interaction between the graphene and CO_2. Conversely, in the GRA-NADES-flue gas systems, the GRA–CO_2 interaction energy is negligible. This can be rationalized by the low partial pressure of CO_2. In this regime, the captured CO_2 molecules are effectively solvated within the bulk liquid and are unlikely to reach the graphene surface. This behavior is further corroborated by the internal interaction analysis (Fig. 10). In the pure GRA-NADES-CO_2 systems, the high adsorbate density leads to competitive CO_2–CO_2 interactions, while in the GRA-NADES-flue gas systems, these interactions vanish due to the spatial isolation of the molecules. Consequently, the stability of CO_2 in the flue gas systems is driven almost exclusively by solvation forces, where MENTH–CO_2 interactions predominate over DA–CO_2 interactions. These profiles remain stable under heating.

Notably, MENTH and DA molecules structuring within the NADES region undergo negligible deviations after CO_2 adsorption, as provided by the $N_{H\text{-bonds}}$ both in the first adsorbed layer and the bulk region (Fig. 4), charge distribution in the region nearby GRA surface (Fig. 5b for pure CO_2 and 5c for flue gas) and molecular orientation inclination towards the GRA flake (Fig. 6b for pure CO_2 and 6c for flue gas). MENTH-GRA and DA-GRA E_{int} after CO_2 adsorption moderately deviate from NADES/vacuum behavior at the different layers thickness induced by the competing effect of CO_2 molecules to adsorb on GRA surface (Fig. 7).

4. Conclusions

A comprehensive molecular-level investigation of graphene-supported menthol–decanoic acid (MENTH:DA) NADES thin films was conducted, combining quantum-mechanics DFT and molecular-mechanics MD simulations to assess interfacial structuring and CO_2 adsorption performance. The adsorption behavior of individual NADES components on graphene surfaces was found to be strongly asymmetric: decanoic acid exhibited substantial interaction energies and parallel orientation with the substrate, while menthol displayed weaker interactions and preferred a perpendicular alignment. These distinct orientations result in stratified interfacial architectures, with decanoic acid preferentially occupying the first adsorbed layer and menthol enriching subsequent layers. Despite local molecular reorganization near the interface, the hydrogen-bonding network characteristic of bulk NADES was largely retained, indicating that the supramolecular structure of the solvent remains robust under confinement. CO_2 molecules showed preferential physisorption in both the first and second interfacial layers of the NADES film, with notable selectivity over N_2, H_2O, and O_2. Under simulated flue gas conditions, approximately 50% of the total CO_2 content was adsorbed within the NADES film. CO_2 maintained a predominantly parallel orientation with respect to the graphene substrate, maximizing van der Waals interactions, and interaction energies remained relatively stable across varying temperatures (303–323 K) and film thicknesses (20–50 Å), underscoring the thermal resilience of the system.

These findings establish a predictive computational framework for the design of graphene-supported, type V NADES-based membranes with high selectivity and affinity for CO_2 under realistic multicomponent gas conditions. The use of natural, non-ionic constituents ensures environmental compatibility and positions these materials as promising candidates for low-cost, metal-free CO_2 capture technologies, especially in membrane separation systems.

Further research should focus on experimental validation of the predicted structural motifs and adsorption trends using surface-sensitive characterization techniques. Long-term performance under cyclic adsorption–desorption conditions, optimization of NADES formulations with alternative monoterpenoid components, and integration onto functionalized or porous graphene architectures represent promising directions. In addition, the exploration of electrochemical or catalytic enhancements to adsorption, as well as technoeconomic analyses of system scalability, are essential for advancing these materials towards industrial deployment.

CRediT authorship contribution statement

Sara Rozas: Writing – review & editing, Writing – original draft, Visualization, Validation, Methodology, Investigation, Formal analysis, Data curation, Conceptualization. **Nuria Aguilar:** Writing – review & editing, Writing – original draft, Visualization, Validation, Investigation, Formal analysis, Data curation, Conceptualization. **Pedro A. Marcos:** Writing – review & editing, Writing – original draft, Visualization, Validation, Methodology, Investigation, Formal analysis, Data curation, Conceptualization. **Alfredo Bol:** Writing – review & editing, Writing – original draft, Visualization, Validation, Supervision, Methodology,

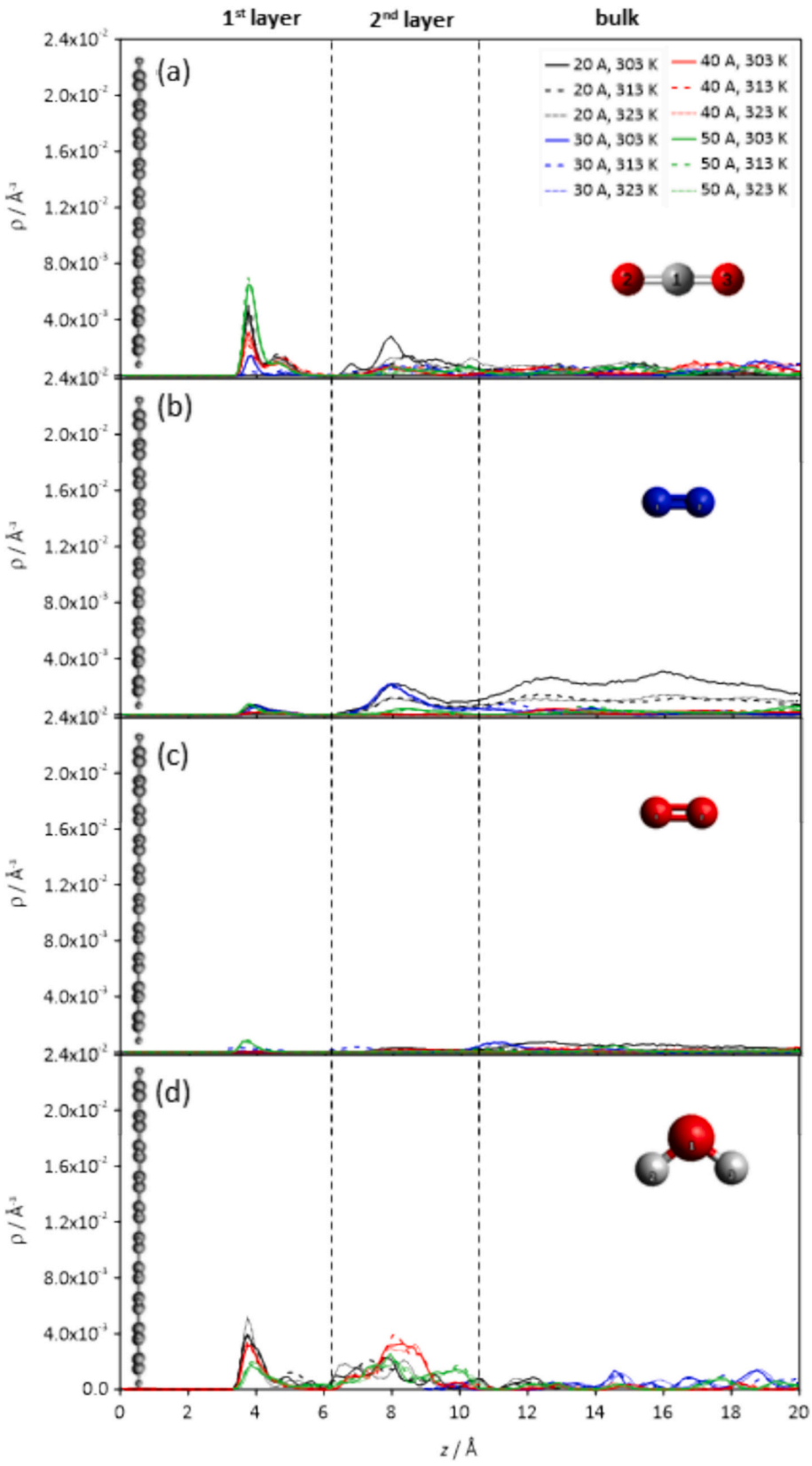

Fig. 9. Number of density profiles, ρ, for the center-of-mass of (a) CO_2, (b) N_2, (c) O_2 and (d) H_2O at the considered temperature and DES film depth conditions as a function of the distance, z, to the GRA surface from MD simulations. Only data in the vicinity of the GRA surface ($z < 20$ Å) is reported. Vertical dashed lines represent first and second adsorbed layers.

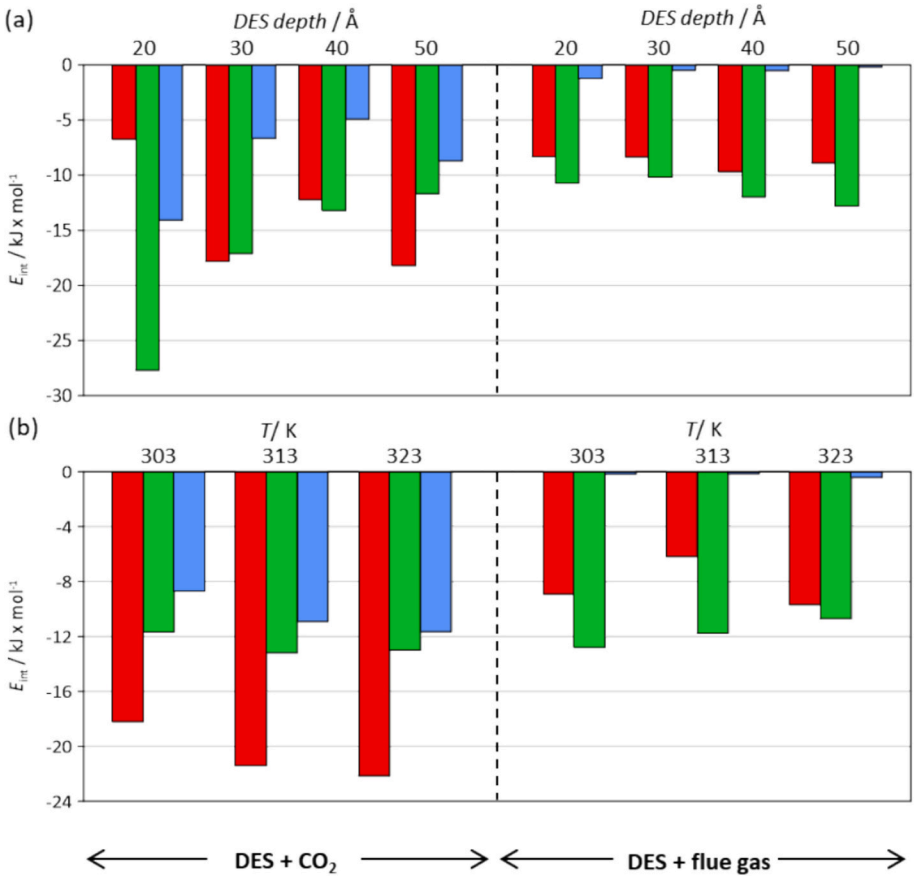

Fig. 10. Interaction energies, E_{int}, for MENTH – CO_2 (red), DA – CO_2 (green) and CO_2 – CO_2 (blue) from MD simulations at (a) 303 K and different DES depths and (b) 50 Å DES depth and different temperatures. GRA – DES + CO_2 and GRA – DES + flue gas systems were considered. (For interpretation of the references to colour in this figure legend, the reader is referred to the web version of this article.)

Investigation, Formal analysis, Data curation, Conceptualization. **Santiago Aparicio:** Writing – review & editing, Writing – original draft, Visualization, Validation, Supervision, Software, Resources, Project administration, Methodology, Investigation, Funding acquisition, Formal analysis, Data curation, Conceptualization.

Declaration of competing interest

None.

Acknowledgements

This work was funded by the European Union (873005-WORLD-H2020-MSCA-RISE-2019). We also acknowledge SCAYLE (Supercomputación Castilla y León, Spain) and COMPUTAEX (Supercomputación Extremadura, Spain) for providing supercomputing facilities. The statements made herein are solely the responsibility of the authors.

Appendix A. Supplementary data

Supplementary material: Fig. S1 (graphene flake used for DFT); Fig. S2 (DFT geometry optimizations of individual species on graphene); Table S1-S8 (Force field parametrization); Table S9 (MD initial configurations); Fig. S3 (DFT optimized structures of monomers adsorbed on GRA); Fig. S4 (Density profiles of MENTH and DA on GRA as a function of DES depth from MD simulations); Fig. S5 (Density profiles of MENTH and DA on GRA as a function of temperature from MD simulations); Table S10 (Number of MENTH and DA molecules in the first adsorption layer).

Data availability

Data will be made available on request.

References

[1] National Oceanic & Atmospheric Administration, U. S. Department of Commerce, Earth System Research Laboratories, accessed 13 March 2025, https://www.noaa.gov/>, 2025.
[2] T. Wilberforce, A.G. Olabi, E.T. Sayed, K. Elsaid, M.A. Abdelkareem, Progress in carbon capture technologies, Sci. Total Environ. 761 (2021) 143203.
[3] S. Sarmad, J.-P. Mikkola, X. Ji, Carbon dioxide capture with ionic liquids and deep eutectic solvents: a new generation of sorbents, Chem. Sus. Chem. Rev. 10 (2017) 324–352.
[4] K. Zhang, Y.C. Hou, Y.M. Wang, K. Wang, S.H. Ren, W.Z. Wu, Efficient and reversible absorption of CO2 by functional deep eutectic solvents, energy, Fuel 32 (2018) 7727–7733.
[5] A. Al-Bodoura, N. Alomari, A. Gutierrez, S. Aparicio, M. Atilhan, High-pressure carbon dioxide solubility in terpene based deep eutectic solvents, J. Environ. Chem. 10 (5) (2022) 108237.
[6] A. Al-Bodoura, N. Alomari, S. Aparicio, M. Atilhan, A comprehensive study on carbon capture potential of lactic acid based deep eutectic solvents at wide process conditions, J. Mol. Liq. 390 (Part B) (2023) 123114.
[7] D. Fuchs, B.C. Bayer, T. Gupta, G.L. Szabo, R.A. Wilhelm, D. Eder, J.C. Meyer, S. Steiner, B. Gollas, Electrochemical behavior of graphene in a deep eutectic solvent, ACS Appl. Mater. Interfaces 12 (36) (2020) 40937–40948.
[8] Z. Chen, B. McLean, M. Ludwig, R. Stefanovic, G.G. Warr, G.B. Webber, A.J. Page, R. Atkin, Nanostructure of deep eutectic solvents at graphite electrode interfaces as a function of potential, J. Phys. Chem. C 120 (4) (2016) 225–2233.

[9] J. Gao, W. Yu, H. Xie, O. Mahian, Graphene-based deep eutectic solvent nanofluids with high photothermal conversion and high-grade energy, Renew. Energy 190 (2022) 935–944.
[10] X. Fan, Z. Zhao, C. Li, X. Li, Y. He, M. Zhu, Deep eutectic solvent intercalation graphene oxide with strong interfacial adsorption capacity towards efficient lubrication, Carbon 216 (2024) 118508.
[11] M. Shakourian-Fard, S.M. Taimoory, H.R. Ghenaatian, G. Kamath, J.F. Trant, A DFT study of the adsorption of deep eutectic solvents onto graphene an defective graphene nanoflakes, J. Mol. Liq. 327 (2021) 114580.
[12] M. Atilhan, L.T. Costa, S. Aparicio, Elucidating the properties of graphene-deep eutectic solvents interface, Langmuir 33 (2017) 5154–5165.
[13] F. Neese, Software update: the ORCA program system, version 5.0, Comput. Mol. Sci. 12 (1) (2022) e1606.
[14] N. Mardirossian, M. Head-Gordon, ωB97X-V: a 10-parameter, range-separated hybrid, generalized gradient approximation density functional with nonlocal correlation, designed by a survival-of-the-fittest strategy, Phys. Chem. Chem. Phys. 16 (2014) 9904–9924.
[15] F. Weigened, R. Ahlrichs, Balanced basis sets of split valence, triple zeta valence and quadrupole zeta valence quality for H to Rn: design and assessment of accuracy, Phys. Chem. Chem. Phys. 7 (2005) 3297–3305.
[16] F. Weigend, Accurate coulomb-fitting basis sets for H to Rn, Phys. Chem. Chem. Phys. 8 (2006) 1057.
[17] S. Rozas, S. Martín-Martel, N. Aguilar, A. Gutiérrez, P.A. Marcos, A. Bol, M. Atilhan, A. Mele, S. Aparicio, An in silico study on the carbon capture performance of menthol-based natural deep eutectic solvent, Fuel 392 (2025) 134784.
[18] S. Simon, M. Duran, J. Dannenberg, How does basis set superposition error change the potential surfaces for hydrogen-bonded dimers? J. Chem. Phys. 105 (1996) 11024–11031.
[19] F.L. Hirshfeld, Bonded-atom fragments for describing molecular charge densities, Theoret. Chim. Acta. 44 (1977) 129–138.
[20] E.R. Johnson, S. Keinan, P. Mori-Sanchez, J. Contreras-García, A.J. Cohen, W. Yang, Revealing noncovalent interactions, Am. Chem. Soc. 132 (2010) 6498–6506.
[21] Lu Tian, F. Chen, Multiwfn: a multifunctional wavefunction analyzer, J. Comput. Chem. 33 (2012) 580–592.
[22] A.P. Lyubartsev, A. Laaksonen, MDynaMix - a scalable portable parallel MD simulation package fro arbitrary molecular mixtures, Comput. Phys. Commun. 1258 (2000) 565–589.
[23] V. Zoete, M.A. Cuendet, A. Grosdidier, O. Michielin, SwissParam: a fast force field generation tool for small organic molecules, J. Comput. Chem. 32 (2011) 2359–2368.
[24] C.M. Breneman, K.B. Wiberg, Determining atom-centered monopoles from molecular electrostatic potentials. The need for high sampling density in formamide conformational analysis, J. Comput. Chem. 11 (1990) 361–373.
[25] S. Aparicio, M. Atilhan, Molecular dynamics study of carbon nanostructures in N-methylpiperazinium lactate ionic liquid, J. Phys. Chem. C 117 (2013) 22046–22059.
[26] J.G. Harris, K.H. Yung, Carbon dioxide's liquid-vapour coexistence curve and critical properties as predicted by a simple molecular model, J. Phys. Chem. 99 (31) (1995) 11797–12064.
[27] C.S. Murthy, K. Singer, M.L. Klein, I.R. McDonald, Pairwise additive effective potentials for nitrogen, Mol. Pysh. 41 (6) (1980) 1387–1399.
[28] L. Martínez, R. Andrade, E.G. Birgin, J.M. Martínez, PACKMOL: a package for building initial configurations for molecular dynamics simulations, J. Comput. Chem. 30 (2009) 2157–2164.
[29] W.G. Hoover, Canonical dynamics: equilibrium phase-space distributions, Phys. Rev. A 32 (1985) 1695–1697.
[30] M. Tuckerman, B.J. Berne, Reversible multiple time scale molecular dynamics, J. Chem. Phys. 97 (1992) 1990–2001.
[31] U.L. Essmann, L. Perera, M.L. Berkowitz, A smooth particle mesh Ewald method, J. Chem. Phys. 103 (1995) 8577–8593.
[32] M. Brehm, B. Kirchner, TRAVIS - a free analyzer and visualizer for Monte Carlo and Molecular dynamics trajectories, J. Chem. Inf. Model. 51 (2011) 2007–2023.
[33] W. Humphrey, A. Dalke, K. Schulten, VMD: Visual molecular dynamics, J. Mol. Graph. 14 (1996) 33–38.
[34] P. Lazar, F. Karlický, P. Jurecka, M. Kocman, E. Otyepková, K. Safárová, M. Otyepka, Adsorption of small organic molecules on graphene, J. Am. Chem. Soc. 135 (2013) 6372–6377.